Closed-form expression for the profile of partially wetting two-dimensional droplets under gravity

J. M. Gomba[1,*] and Carlos Alberto Perazzo[2,†]

[1]*Department of Mechanical Engineering, University of California, Santa Barbara, California 19327, USA*

[2]*Departamento de Física y Química, Universidad Favaloro, Solís 453, 1078, Buenos Aires, Argentina*

(Received 13 June 2012; revised manuscript received 26 September 2012; published 19 November 2012)

Analytical solutions for the shape of both hanging and sitting droplets under the effects of gravity and surface tension are presented. The modeling also includes the action of molecular forces arising between the liquid and the substrate, which are responsible for the formation of a stable nanometric film in the region close to the droplet contact line. The shape of the droplet is completely described by an analytical solution that also accounts for the pancake-shaped droplets as a limiting case. We find expressions that relate microscopic and nanoscopic aspects, such as the strengths of the molecular forces and the thickness of the nanometric film, to macroscopic quantities, such as the cross-sectional area and the width of the droplet. We study the effect of gravity on the contact angle and find that for small droplets the contact angle follows a power law with the droplet's size. For sitting droplets we find that the there is an upper limit for the value of the gravity.

DOI: 10.1103/PhysRevE.86.056310 PACS number(s): 47.55.np, 47.55.dr

I. INTRODUCTION

The study of the shape of droplets offers a large number of research opportunities both in fundamental and applied fields. On the fundamental side, the dynamics and statics of droplets are now possible to experimentally explore at the nanometric scale thanks to the development of new techniques on droplet production and imaging. This information is useful to test theoretical models that relate geometric and molecular parameters and also to improve the understanding of wetting related phenomena, such as the coarsening and coalescence of droplets, the dependence of contact angle on droplets size and temperature, line tension effects, volume selection, contact line instabilities, etc. [1–19]. From the technological side, this field of research is increasing our understanding of key processes of printing, coating, and electronic industries [20–24]. The knowledge of the dynamics of wetting developed during the last two decades also has crucial importance to the design of a large number of microfluidic devices [25], and more research on this issue is needed in order to improve the efficiency of these reduced-size systems, where the action of interfacial and molecular forces play a key role.

Here, we present analytical solutions for the thickness profile of hanging and sitting two-dimensional droplets under partially wetting conditions. The modeling takes into account capillary and gravity effects as well as the forces between the liquid and solid molecules. Following Derjaguin [26], the integrated action of attractive and repulsive molecular forces results in a net disjoining-conjoining pressure. Although this pressure must be considered only when the fluid thickness goes below 100 nm, its effect has a large impact on the wetting properties of the fluid and thus on the macroscale dynamics of droplets and films [3,9,27].

In general, three different regions can be distinguished in the shape of a large droplet. The first one is the bulk, where the effect of the intermolecular forces is negligible and the thickness profile is the result of the action of the capillarity and gravity (if considered). The second region is constituted by a constant-thickness nanometric film that surrounds the droplet, where the thickness is determined by the competition of intermolecular forces between the solid and the liquid. The last one is the transition region, where the bulk meets the nanometric film and where all the involved forces compete [28–30]. Different methods have been applied to describe the shape of these three regions, such as the numerical resolution of the governing equations [31], asymptotic matching [30,32], series expansions, which is valid in the region where the liquid-vapor interface meets the substrate [27,33,34], guess functions [35], and parametric solutions [36].

Despite the large number of papers analyzing the morphology of droplets, few of them give analytical solutions that relate the macroscopic and microscopic parameters of the droplets when a pair of attractive and repulsive molecular forces are considered. To our knowledge, the first complete analytical solution was reported in Ref. [37], in which the gravity was not included in the model. In that work, the authors find a unique expression for the complete profile of the droplet and present a number of analytical results that link molecular and shape parameters. Here, we extend their study by including the effect of gravity, finding solutions and analyzing some restrictions that gravity imposes on them.

This article is organized as follows. In Sec. II we introduce the formulation. In Sec. III we analyze the range of parameters for which the governing equation has an analytical solution with the shape of a drop. The analytical solutions for the thickness profile of the droplet and for its cross-sectional area are presented in Sec. IV, while the effect of gravity on the contact angle is analyzed in Sec. V. Finally, the last section is devoted to the conclusions.

II. FORMULATION

In this section we introduce the basic equations. Although we focus on stationary droplets, here we include temporal terms in order to show that the proposed adimensionalization results in a one-parameter dimensionless equation even when

*Present address: Instituto de Física Arroyo Seco, Universidad Nacional del Centro de la Provincia de Buenos Aires, Pinto 399, 7000, Tandil, Argentina; jgomba@engr.ucsb.edu

†perazzo@favaloro.edu.ar

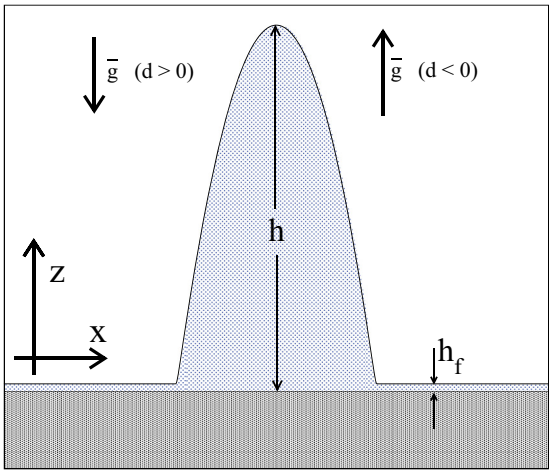

FIG. 1. (Color online) Scheme of a sitting ($d > 0$) or hanging ($d < 0$) droplet. Here, h_f is the thickness of the precursor film that surrounds the droplet.

nonstationary droplets are considered. We analyze the case of a two-dimensional droplet sitting on (or hanging from) a horizontal rigid substrate, as shown in Fig. 1.

The liquid is Newtonian, with a viscosity μ, density ρ, and coefficient of surface tension γ. The horizontal and the vertical coordinates are x and z, respectively, and t is the time. The thickness of the film is $h \equiv h(x,t)$, and we assume that the slope of the free surface is gentle and the flow is slow. With these assumptions we can apply the lubrication approximation [13,38], so that the evolution of h is governed by

$$\frac{\partial h}{\partial t} + \frac{\partial (uh)}{\partial x} = 0, \quad u = -\frac{1}{3\mu} h^2 \frac{\partial p}{\partial x}, \tag{1}$$

with [39]

$$p = -\gamma \frac{\partial^2 h}{\partial x^2} + \rho g(h - z) - \Pi(h) + \Pi(z). \tag{2}$$

Here u is the vertically averaged horizontal velocity, and g is the acceleration due to gravity. The pressure p has three contributions: the Laplace pressure, the hydrostatic pressure, and the conjoining-disjoining pressure Π, which we choose as [14,40]

$$\Pi(h) = \kappa \left[\left(\frac{h_0}{h} \right)^n - \left(\frac{h_0}{h} \right)^m \right], \tag{3}$$

where $n > m$, h_0 is an energetically favored molecular thickness, and κ is related to the Hamaker constant [37].

Defining the dimensionless variables and quantities,

$$\widehat{h} = h/h_0, \quad \widehat{x} = x/x_0, \quad \widehat{t} = t/t_0, \quad \widehat{u} = u\, t_0/x_0, \tag{4}$$

and choosing $x_0^2 = \gamma h_0/\kappa$ and $t_0 = 3\mu\gamma/h_0\kappa^2$, the evolution equations for the dimensionless thickness become

$$\frac{\partial h}{\partial t} + \frac{\partial (uh)}{\partial x} = 0, \tag{5}$$

$$u = h^2 \frac{\partial}{\partial x} \left[\frac{\partial^2 h}{\partial x^2} + \left(\frac{1}{h^n} - \frac{1}{h^m} \right) - dh \right], \tag{6}$$

where we have omitted the hats for simplicity. Notice that with this scaling d is the unique parameter of the governing equation, and it is given by

$$d \equiv \frac{\rho g h_0}{\kappa} = \frac{\rho g x_0^2}{\gamma}. \tag{7}$$

This dimensionless number quantifies the relative strength of gravity with respect to the molecular interaction between the solid and the liquid. The case of droplets hanging from a substrate is analyzed by considering $d < 0$.

To look for stationary solutions for Eqs. (5) and (6) we impose $u = 0$ to get

$$h'' + \left(\frac{1}{h^n} - \frac{1}{h^m} \right) - dh = -P, \tag{8}$$

where each prime denotes a derivative with respect to x and P is a constant to be determined. The solution we are seeking tends to a nanometric flat film h_f for $x \to \pm\infty$, a boundary condition that allows us to write P in terms of h_f:

$$P = -\left(\frac{1}{h_f^n} - \frac{1}{h_f^m} \right) + dh_f. \tag{9}$$

Substituting Eq. (9) in Eq. (8), we obtain

$$0 = h'' + \left(\frac{1}{h^n} - \frac{1}{h^m} \right) - \left(\frac{1}{h_f^n} - \frac{1}{h_f^m} \right) - d(h - h_f). \tag{10}$$

The integration of this last equation results in

$$0 = \frac{1}{2}(h')^2 + \left(\frac{1}{1-n}\frac{1}{h^n} + \frac{1}{m-1}\frac{1}{h^m} \right) h - \left(\frac{1}{h_f^n} - \frac{1}{h_f^m} \right) h - \frac{1}{2} dh^2 + dh_f h + C. \tag{11}$$

The value of C is found from the condition $h' \to 0$ for $h \to h_f$. Finally, we assume, as in Ref. [37] and the references therein, $n = 3$ and $m = 2$ to find out h':

$$(h')^2 = \frac{(h - h_f)^2}{h^2 h_f^3} \left[dh^2 h_f^3 - 2(h_f - 1)h + h_f \right]. \tag{12}$$

It is instructive to observe that Eq. (12) can also be obtained by minimizing the dimensionless energy

$$F(h,h') = \int (u_g + u_\Pi + u_\gamma) dx, \tag{13}$$

where

$$u_g = \frac{1}{2} dh^2, \tag{14}$$

$$u_\Pi = \frac{1}{2h^2} - \frac{1}{h}, \tag{15}$$

$$u_\gamma = \frac{1}{2} h'^2. \tag{16}$$

For a vertical column of fluid with height h and width dx, the above defined u_g, u_Π, and u_γ are the gravitational energy, the energy from the molecular interaction with the substrate, and the energy from surface tension, respectively.

III. PARAMETER SPACE ANALYSIS

In this section we analyze the values of h_f and d for which Eq. (12) allows a droplet solution. The solution must verify two conditions. The first one is that it must have two values of h for which $h' = 0$; one of them is h_f, and the other corresponds to the maximum of the profile h_m. Naturally, the second condition is that $h_m > h_f$.

Besides $h = h_f$, h' has two other roots. One of them has no physical sense, and the second one, corresponding to the maximum of the droplet, is

$$h_m = \frac{h_f - 1 - \sqrt{(h_f-1)^2 - d h_f^4}}{d h_f^3}. \tag{17}$$

In order to ensure a real value, the second order polynomial within the square root in Eq. (17) must be non-negative. This condition gives a first restriction to the value of d:

$$d \leqslant d_* \equiv \frac{(h_f-1)^2}{h_f^4}. \tag{18}$$

The second condition, which is to impose that $h_m > h_f$, gives

$$d_{\min} < d < d_{\max} \quad \text{for} \quad 0 < h_f \leqslant 2, \tag{19}$$

where

$$d_{\min} \equiv \frac{2h_f - 3}{h_f^4},$$
$$d_{\max} \equiv \begin{cases} 0 & \text{for} \quad 0 < h_f \leqslant 1, \\ d_* & \text{for} \quad 1 < h_f \leqslant 2. \end{cases} \tag{20}$$

Figure 2 shows the region of the space parameter where the condition given in Eq. (19) is verified. Observe that for a fixed d we have $h_{f,\min} \leqslant h_f \leqslant h_{f,\max}$, where

$$h_{f,\min} = \begin{cases} 0 & \text{if} \quad d < 0, \\ \frac{2}{1+\sqrt{1-4\sqrt{d}}} & \text{if} \quad d \geqslant 0, \end{cases} \tag{21}$$

and

$$h_{f,\max} = \frac{D}{2}\left(\sqrt{r} - \sqrt{-r + D\frac{4}{d\sqrt{r}}}\right). \tag{22}$$

Here $D \equiv \operatorname{sgn}(d)$, and r is given by

$$r \equiv \frac{2^{5/3} d + 2^{1/3}(d + \sqrt{d^2 - 16d^3})^{2/3}}{d(d + \sqrt{d^2 - 16d^3})^{1/3}}. \tag{23}$$

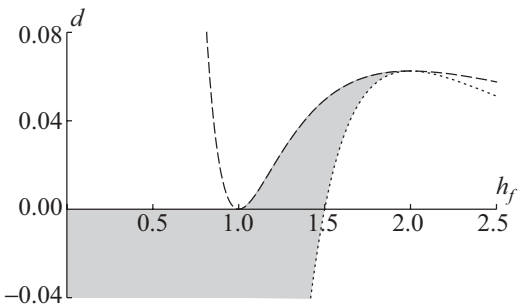

FIG. 2. The gray zone represents the values of d and h_f for the existence of droplet solutions. The dashed line is $d = d_*$, and the dotted one is $d = d_{\min}$.

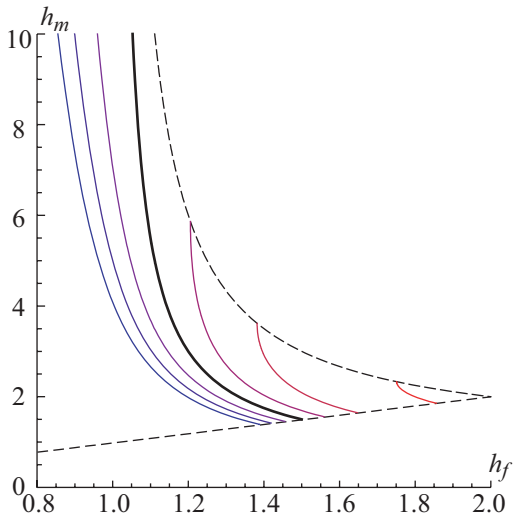

FIG. 3. (Color online) The maximum thickness h_m given by (17) as function of h_f for $d = 0, \pm 0.02, \pm 0.04$, and ± 0.06. The parameter d increases from left to right (from blue to red). The thick line corresponds to $d = 0$, and the dashed lines correspond to $h_m = h_f$ and $h_m = h_m^*$.

From Eq. (21), the maximum value for d is $1/16$, which corresponds to $h_f = 2$.

Figure 3 shows the maximum thickness of the droplet h_m for different values of d. Notice that for a given $d > 0$ (sitting droplets), h_m has an upper bound h_m^* given by

$$h_m^* = \frac{h_{f,\min}}{(h_{f,\min} - 1)} \equiv \frac{2}{1 - \sqrt{1 - 4\sqrt{d}}}. \tag{24}$$

As expected, for nongravity conditions or hanging droplets, i.e., $d \leqslant 0$, h_m is unbounded.

IV. THE ANALYTICAL THICKNESS PROFILE

In this section we present an analytical expression that describes completely the thickness profile of a droplet from the nanometric precursor film to the maximum. We also analyze how the involved parameters affect the shape of the droplet.

Equation (12) can be integrated to obtain the solution of the thickness profile in the following implicit form:

$$x = -\frac{1}{\sqrt{d}} \ln\left(\frac{s_1 - s\sqrt{d}}{h_f\sqrt{d_{\max} - d}}\right) + \frac{1}{\sqrt{d - d_{\min}}} \times \ln\left(\frac{s_2 + s\sqrt{d - d_{\min}}}{(h - h_f)\sqrt{d_{\max} - d}}\right), \tag{25a}$$

where

$$s = \sqrt{h_f\left(2h + h_f - 2hh_f + dh^2h_f^3\right)},$$
$$s_1 = 1 - \left(1 + dhh_f^3\right)/h_f, \tag{25b}$$
$$s_2 = -1 + \left(h + 2h_f - hh_f + dhh_f^4\right)/h_f^2.$$

Here, without loss of generality, the droplet has been centered at $x = 0$. This solution describes the shape of a droplet for any allowed pair of values of d and h_f. The thickness profile for $d = 0$ presented in Ref. [37] is recovered from Eqs. (25) when d tends to 0.

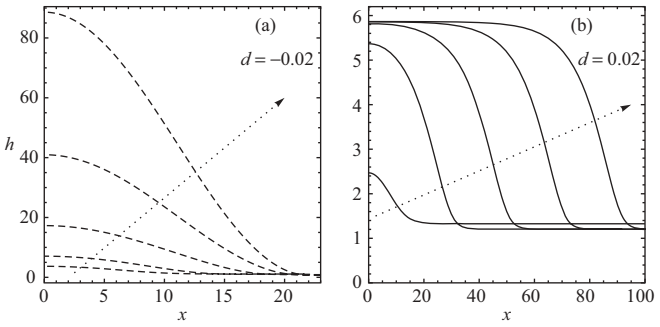

FIG. 4. Thickness profiles for $d =$ const and different values of h_f: (a) $d = -0.02$ and $h_f = 0.7, 0.8, 0.9, 1.0$, and 1.1; (b) $d = 0.02$ and $h_f/h_{f,\min} - 1 = 10^{-1}, 10^{-3}, 10^{-5}, 10^{-7}$, and 10^{-9}. The solid (dashed) lines are for $d > 0$ ($d < 0$). The arrows point in the direction of decreasing h_f.

It is convenient to make a comment about the validity of the solution (25). Notice that Eqs. (1) and (2) were derived assuming the lubrication approximation, which means that the slope of their solutions has to be small. Then, only when this condition is verified does the solution (25) properly describe a droplet. In connection with this, Ref. [41] presents solutions of the Navier-Stokes equations that agree very well with the respective solutions obtained using the lubrication approximation for slopes as large as 30°.

Figure 4 shows the solution presented in Eq. (25) for a negative and a positive value of d and different values of h_f. For a given d, a lower value of h_f corresponds to a larger cross-sectional area a of the droplet. Nevertheless, while for $d < 0$ the increment of the area is carried out by continuously increasing h_m, for $d > 0$ we have that, as $h_f \to h_{f,\min}$ (and then $h_m \to h_m^*$), the area is instead incremented by increasing its width. This last case corresponds to the "pancake"-shaped droplet [9], a profile that is completely described as a limit case of Eq. (25) without the need of assuming a strictly flat profile (null first derivative) at the top of the droplet.

A similar analysis can be performed by keeping h_f constant and changing d continuously. Figure 5 shows profiles of droplets for $h_f < 1$ (for which $d_{\max} = 0$) and $h_f > 1$. In the first case, when d is increased from $d_{\min}$ to $d_{\max}$, the area of the droplet continuously grows from zero to infinite by increasing

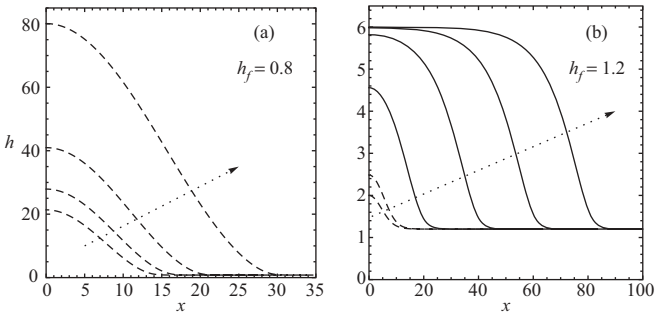

FIG. 5. Thickness profiles for $h_f =$ const and different values of d: (a) $h_f = 0.8$ and $d = -0.04, -0.03, -0.02$, and -0.01; (b) $h_f = 1.2$ and $d/d_{\max} - 1 = -3, -2, -10^{-1}, -10^{-3}, -10^{-5}$, and -10^{-7}. The solid (dashed) lines are for $d > 0$ ($d < 0$). The arrows point in the direction of increasing d.

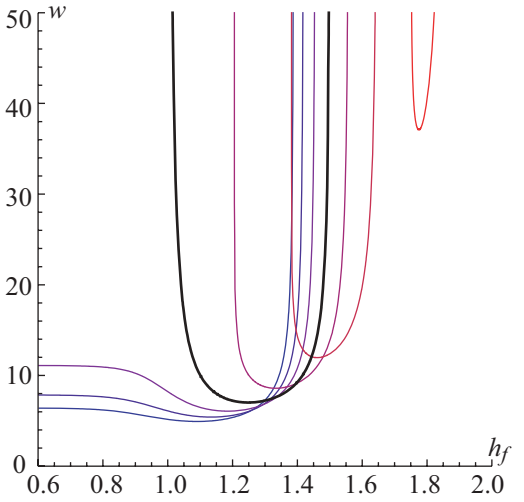

FIG. 6. (Color online) The half width w as function of h_f for $d = 0, \pm 0.02, \pm 0.04$, and ± 0.06. The thick line corresponds to $d = 0$.

h_m. For $h_f > 1$, the area also grows from zero to infinite, but when $d \to d_{\max}$ one has $h_m \to h_m^*$, and the area of the droplet continues growing by increasing its width, in a similar manner as observed for the case with $d =$ const.

We also analyzed the behavior of the half width w of the droplet, arbitrarily defined as

$$w = x\left(\frac{h_f + h_m}{2}\right). \tag{26}$$

From Eqs. (17), (25), and (26) it is possible to obtain a closed expression for w as a function of h_f and d (not shown here for brevity). Figure 6 shows w as a function of h_f for different values of d. Notice that for any fixed d, w has a minimum at some intermediate value between $h_{f,\min}$ and $h_{f,\max}$.

For h_f approaching $h_{f,\min}$ or $h_{f,\max}$, w presents different behaviors depending on the value of d. The half width diverges when $h_f \to h_{f,\max}$ for both positive and negative d and also when $h_f \to h_{f,\min}$ for $d \geqslant 0$. Interestingly, when $h_f \to h_{f,\min}$ and $d < 0$, the half width w tends to a constant, $w_* = \pi/2\sqrt{-d}$ despite h_m tending to infinity, as shown in Fig. 3.

Up to this point, all the presented solutions depend on d and on the nanoscopic parameter h_f. We now introduce the relationship of the cross-sectional area a to the parameters h_f and d, which helps to link all the previously derived solutions with a.

We define the dimensionless area a of the droplet as

$$a = \int_{-\infty}^{\infty} (h - h_f)dx. \tag{27}$$

A close expression for a is obtained by using Eq. (25) and is given by

$$a = -\frac{2}{d}\sqrt{d - d_{\min}}h_f + \frac{2}{h_f^2 d^{3/2}}\left(\frac{1}{h_f} - 1\right) \times \ln\left[\frac{h_f - 1 - dh_f^4 - \sqrt{d(d - d_{\min})}h_f^4}{\sqrt{d_{\max} - d}h_f^2}\right]. \tag{28}$$

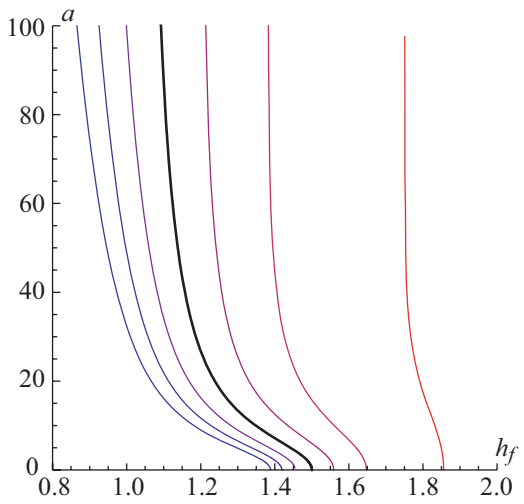

FIG. 7. (Color online) The area a as function of h_f for $d = 0$, ± 0.02, ± 0.04, and ± 0.06 (d increases from left to right). The thick line corresponds to $d = 0$.

Figure 7 shows a as a function of h_f for different values of d. For a fixed d the area is a decreasing function of h_f, ranging from infinity to zero as h_f goes from $h_{f,\min}$ to $h_{f,\max}$.

V. THE CONTACT ANGLE

We define the macroscopic contact angle θ as the slope of the surface $h(x)$ at the inflection point. A closed expression of θ as a function of h_f and d is obtained from Eq. (12), which is given by the roots of a third order polynomial. Thus, three expressions of θ are found, but only one is physically meaningful for given values of h_f and d (the resulting relationships are too long to be written out here). Figure 8 shows θ as function of a for different d. For small a the contact angle verifies $\theta \propto a^3$, where the constant of proportionality depends on d. For large areas, θ is independent of d for $d \leqslant 0$: θ tends to $\pi/2$ for any $d < 0$ and to $\pi/4$ if $d = 0$. For $d > 0$, θ tends to $\theta_{\max}$, a decreasing function of d given by

$$\tan\theta_{\max} = \sqrt{1 - 4d^{1/4} + 4\sqrt{d}}. \tag{29}$$

For sessile drops, when the area is large, the drop adopts the pancake shape. Then, expression (29) gives the contact angle of a pancake droplet. Finally, it is important to remark that Θ, the contact angle of the droplet with the dimensions restored, is related to θ by means of the relationship $\tan\Theta = \sqrt{h_0\kappa/\gamma}\tan\theta$, as was explained in Ref. [37].

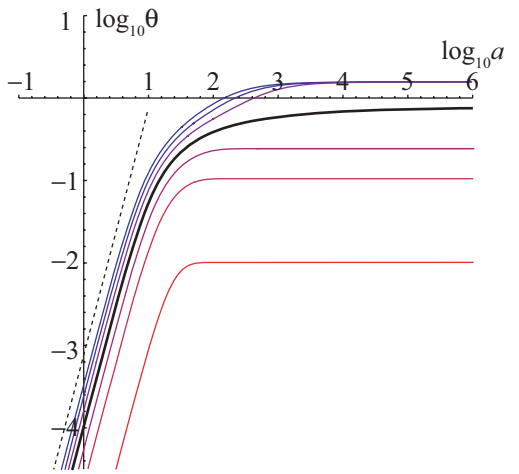

FIG. 8. (Color online) The apparent contact angle θ as function of area a for $d = 0$, ± 0.02, ± 0.04, and ± 0.06. The thick line corresponds to $d = 0$, and the dotted line corresponds to $\theta \propto a^3$.

VI. DISCUSSION AND CONCLUSIONS

In Ref. [37] the case without gravity ($d = 0$) was extensively studied and discussed, so that here we focus attention on the effects of gravity on the characteristics of a droplet. We first discussed the conditions for the existence of a droplet. From Fig. 2, the precursor film h_f of a sessile droplet verifies $1 \leqslant h_{f,\min} < h_f < h_{f,\max} \leqslant 2$, and more remarkable, independently of the value of h_f there is no sessile droplet when $d \geqslant 1/16$ or, equivalently, when $g \geqslant \kappa/16\rho h_0$. For pendant droplets, the thickness of the precursor film satisfies $h_f < h_{f,\max} \leqslant 3/2$, and there is no limit for d, the parameter that measures gravity. Without gravity the condition for the existence of a droplet is $1 \leqslant h_f \leqslant 3/2$, and the comparison with the case for $d > 0$ implies that gravity reduces the range of possible values of h_f and shifts it to larger values. In the case of hanging droplets the presence of gravity allows the existence of droplets with $h_f < 1$.

Some of the requirements for the existence of a droplet, shown in Fig. 2, can be understood in terms of the stability of an infinite film of thickness h_f. This is due to the fact that the droplet may be considered as being mounted over a film with a constant thickness h_f. Effectively, the system of Eqs. (1) and (2) has $h = h_f = \text{const}$ as a solution, and it is straightforward to verify that such a solution is linearly stable for $d > d_{\min}$, with $d_{\min}$ defined in Eq. (20). In a similar way, when the linear stability of a flat film is studied for a given d, it is easy to find that the film is stable only when $h_f \leqslant h_{f,\max}$, with $h_{f,\max}$ given in Eq. (22). Thus, some of the requirements for the existence of a droplet are just the necessary conditions for the stability of the film that surrounds the droplet.

For the existence of a thin film with thickness h_f it is also required that the surface energy of the dry substrate is larger than the surface energy of the substrate covered with the film:

$$\gamma_{SV} \geqslant \gamma_{\text{film}}, \tag{30}$$

where γ_{SV} is the surface tension of the unwetted substrate and γ_{film} is the effective surface tension of a film, and it is given by [39]

$$\gamma_{\text{film}} = \gamma + \gamma_{SL} + h_0\kappa\left[u_\Pi(h_f) + \frac{h_f}{\kappa}\Pi(h_f) - \frac{1}{2}dh_f^2\right].$$

Here γ_{SL} is the surface tension of the solid-liquid interface. Replacing this expression in Eq. (30) and introducing the spreading parameter $S = \gamma_{SV} - (\gamma + \gamma_{SL})$, we obtain

$$\frac{S}{h_0\kappa} \geqslant u_\Pi(h_f) + \frac{h_f}{\kappa}\Pi(h_f) - \frac{1}{2}dh_f^2. \tag{31}$$

Employing the terminology introduced by de Gennes *et al.* [39], the disjoining pressure we are using describes a

pseudopartial wetting. In particular, in our case $\Pi \to \infty$ as $h \to 0$, and therefore we are dealing with a spreading parameter $S = \infty$. Henceforth Eq. (31) is satisfied for any combination of the parameters h_f and d. Only if we slightly modify our disjoining pressure in a way that S becomes finite, but still positive, will Eq. (31) imply a new minimum for h_f only when $d < 0$.

Figure 3 shows that when gravity is absent, the maximum height h_m of a droplet has no upper bound. But for a given value $d > 0$ the value of h_m has an upper bound given by Eq. (24). This means that gravity limits the height of a droplet on a substrate. On the other hand, for a given $d < 0$ the behavior of h_m is similar to the case with $d = 0$.

Regarding the half width w, Fig. 6 shows that for a given value $d \geqslant 0$ there is a minimum value. As d increases, this minimum also increases, and it occurs at larger values of h_f.

It is interesting to note that the increment of the area is achieved in three different ways. In the first one, the area is increased by growing h_m and keeping its width w constant. This case occurs for $d = \text{const} < 0$ when $h_f \to 0$. In the second one, both h_m and w grow, a behavior observed for $h_f = \text{const} < 1$ when $d \to 0$. In the third case, the maximum height h_m is kept constant and only w is increased. This last way to grow the area of the droplet occurs for $d > 0$ and $h_f \to h_{f,\min}$. These different ways to increase the area are based on a minimization of the energy. For example, for the case of a sessile droplet placed on a substrate ($d > 0$) and when its area is very large (i.e., in the limit $h_f \to h_{f,\min}$ or $d \to d_{\max}$), any added mass is energetically more easily located by increasing the width of the droplet and keeping its height constant [notice from Eq. (14) that the gravitational energy grows as h^2]. On the contrary, for the case of a hanging droplet ($d < 0$), when the area is increased, the gravity tends to stretch the droplet in the vertical direction (when $d < 0$, the gravitational energy decreases as h^2).

Another remarkable difference between hanging and sitting droplets is the dependence of θ with d. Figure 8 shows that for a sitting droplet and considering its area a as a constant, the contact angle decreases as the absolute value of gravity becomes larger. For the case of a pendant droplet the behavior is the opposite.

For a droplet with a nanoscopic precursor film a contact angle Θ^* can be defined from the equilibrium condition of the horizontal forces, which leads to $\gamma \cos\Theta^* = \gamma_{\text{film}} - \gamma_{\text{SL}}$. Notice that this definition assumes that the thickness of the drop is much larger than the thickness of the precursor film so that a clear transition between the drop and the film exists. The contact angle θ adopted in this work (defined as the angle at the inflection point) agrees with Θ^* only when $d \to 0$ and $h_f \to 1$. This can be understood by noting that in this limit the maximum thickness h_m of the droplet tends to infinity. The thickness of the droplet diverges also when $d < 0$ and $h_f \to 0$, but in this case the contact angle θ tends to $\pi/2$ (see Fig. 8), so that the gentle slope condition $h' \ll 1$ is not verified.

The stability analysis of thin films and droplets has been addressed elsewhere [30–32,42,43]. In those works, the authors found that an unstable film first breaks up into near-equilibrium droplets connected by an ultrathin film. This stage is followed by a slow coarsening process, in which the droplets exchange mass with neighbors through the thin film. The rate of coarsening depends on whether gravity is included or not. When gravity is not considered, the number of droplets $N(t)$ follows a $t^{-2/5}$ power law [30]. When gravity is not negligible, the number of droplets decrease as $N(t) \propto 1/\ln t$ [32]. The final stage consists of a single droplet in equilibrium with a surrounding thin film. This final configuration is stable, and it is the situation described by our solution. This fact, of course, does not allow us to claim that our solution is stable for all the allowed combinations of parameters h_f and d. Although the goal of this paper is to present analytical solutions describing this final situation and a complete stability analysis is out of the scope of this work, we illustrate in the Appendix how an unstable configuration evolves to our analytical solution.

Finally, notice that the solution given in Eq. (25) also describes the transversal profile of an infinite straight rivulet flowing down over or below a rigid inclined plane after replacing g by $g\cos\alpha$, where α is the angle between the substrate and the horizontal. In this case the velocity is parallel to the plane, and its profile is obtained by resolving a Poisson equation [41,44].

In summary, a complete analytical solution for the shape of a droplet under the effects of gravity, surface tension, and solid-fluid molecular forces was presented. With this solution it is possible to analyze the connection between the thickness of the precursor film and gravity with the characteristics of a droplet, such as height, width, area, and contact angle. This solution describes, for example, the pancake-shaped droplet, a profile analyzed by many authors but for which no analytical solution has been reported [38,39].

ACKNOWLEDGMENTS

C.A.P. and J.M.G. acknowledge Grants PIP No. 299 and PIP No. 356, respectively, both from Consejo Nacional de Investigaciones Científicas y Técnicas (CONICET).

APPENDIX: EVOLUTION TO THE STEADY STATE

We here show how a nonsteady configuration evolves to the analytical solution given by Eq. (25a). Knowing the initial volume A, is it possible to predict the final thickness of the precursor film h_f and thus predict the final area of the droplet, its maximum, etc. In order to determine the stationary value for h_f, we equate the initial volume and the final volume (unknown), that is,

$$A = a + L \times h_f, \tag{A1}$$

where $a = a(h_f, d)$ is given by Eq. (28) and L is the numerical domain.

We solve numerically the evolution equation for h, i.e., the dimensionless version of Eq. (1). The boundary conditions at the borders of the numerical domain are $h_x = h_{xxx} = 0$ (no flux condition). The evolution equation is discretized in space by centered finite differences and evolved in time using a Crank-Nicolson time-marching scheme. A complete description of the numerical method employed can be found elsewhere [14,45].

As was largely studied by Witelski and collaborators [30,32], the evolution of a volume of fluid to its steady state

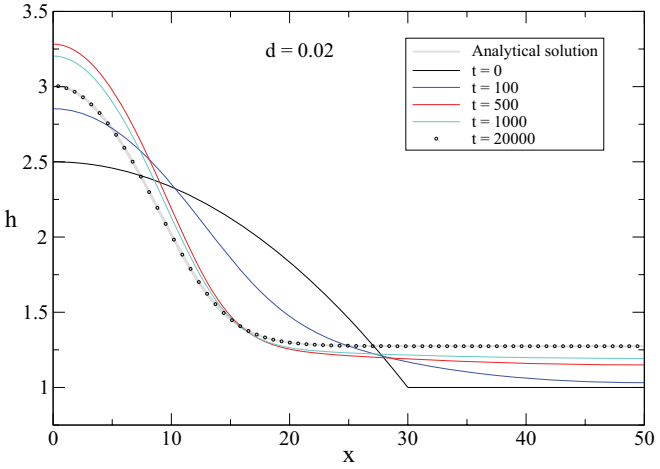

FIG. 9. (Color online) Evolution to the steady state configuration for $d = 0.02$ and $A = 160$. The gray line is the analytical solution, which is reached at $t = 20\,000$.

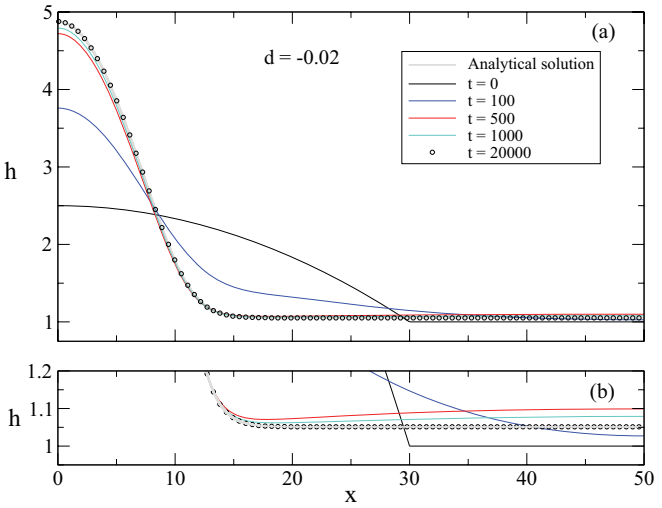

FIG. 10. (Color online) (a) Evolution to a steady state solution for $d = -0.02$ and $A = 160$. The gray line is the analytical solution. (b) A close-up of the precursor film region.

depends on how the mass is initially distributed. But, as explained in the text, they found that nonsteady configurations evolve to a single droplet configuration. Here, we choose an initial distribution of mass that is close to the steady state in order to capture how the bulk and film regions evolve to the analytical solution given by Eq. (25a). The initial area and thickness of the precursor film are $A = 160$ and $h_{f,i} = 1$, respectively.

Figure 9 shows the evolution for $d = 0.02$. By using the mass conservation criteria given in Eq. (A1), the final film thickness is $h_f = 1.27416$. We employ this value to plot the analytical solution in Fig. 9. The corresponding predicted values for the maximum of the droplet and for the cross-sectional area are $h_m = 3.00518$ and $a = 32.58$, respectively, which are in excellent agreement with the numerical simulation. Figure 9 shows that for $t = 20\,000$ the simulation has reached its steady state. We continued the simulation up to $t = 200\,000$, but the profile did not change.

Notice that the profile tries first to match the pressure in the precursor film by increasing its height and curvature. After an abrupt initial increase in the height, it starts to decrease until it reaches the value given by Eq. (17). On the other hand, the thickness of the precursor monotonically reaches the value predicted, $h_f = 1.27416$.

Figure 10 shows the evolution for a hanging droplet with $d = -0.02$. By using the mass conservation criteria given in Eq. (A1), the final film thickness is $h_f = 1.05109$, which is employed to plot the analytical solution in the Fig. 10. Again, the predicted values for the maximum of the droplet and for the cross-sectional area are in excellent agreement with the numerical simulation, as shown in Fig. 10.

For this case, the evolution to the steady state is different from that previously analyzed. Here, the maximum thickness is reached monotonically, while the thickness of the precursor film shows an increase before its thickness is reduced to the final value of h_f.

[1] J. T. Lin and Y. H. Pao, Annu. Rev. Fluid Mech. **11**, 317 (1979).
[2] V. Mitlin and N. V. Petviashvili, Phys. Lett. A **192**, 323 (1994).
[3] U. Thiele, M. G. Velarde, K. Neuffer, and Y. Pomeau, Phys. Rev. E **64**, 031602 (2001).
[4] J. Eggers, Phys. Rev. E **72**, 061605 (2005).
[5] J. M. Gomba, J. Diez, A. G. González, and R. Gratton, Phys. Rev. E **71**, 016304 (2005).
[6] L. Yang and G. M. Homsy, Phys. Fluids **19**, 044101 (2007).
[7] T. Pompe, Phys. Rev. Lett. **89**, 076102 (2002).
[8] J. Y. Wang, S. Betelu, and B. M. Law, Phys. Rev. Lett. **83**, 3677 (1999).
[9] P. G. de Gennes, Rev. Mod. Phys. **57**, 827 (1985).
[10] J. M. Gomba, J. Diez, R. Gratton, A. G. González, and L. Kondic, Phys. Rev. E **76**, 046308 (2007).
[11] A. G. González, J. Diez, R. Gratton, and J. Gomba, Europhys. Lett. **77**, 44001 (2007).
[12] S. Mukhopadhyay and R. Behringer, J. Phys. Condens. Matter **21**, 464123 (2009).
[13] R. V. Craster and O. K. Matar, Rev. Mod. Phys. **81**, 1131 (2009).
[14] J. M. Gomba and G. M. Homsy, J. Fluid Mech. **647**, 125 (2010).
[15] E. R. Jerison, Y. Xu, L. A. Wilen, and E. R. Dufresne, Phys. Rev. Lett. **106**, 186103 (2011).
[16] N. Savva and S. Kalliadasis, Europhys. Lett. **94**, 64004 (2011).
[17] V. S. Ajaev, E. Y. Gatapova, and O. A. Kabov, Phys. Rev. E **84**, 041606 (2011).
[18] G. McHale, C. V. Brown, M. I. Newton, G. G. Wells, and N. Sampara, Phys. Rev. Lett. **107**, 186101 (2011).
[19] S. Mukhopadhyay, N. Murisic, R. P. Behringer, and L. Kondic, Phys. Rev. E **83**, 046302 (2011).
[20] V. Starov, M. Velarde, and C. Radke, *Wetting and Spreading Dynamics, Surfactant Science Series* (CRC Press, Boca Raton, FL, 2007).

[21] P. Y. Paik, V. K. Pamula, and K. Chakrabarty, *Adaptive Cooling of Integrated Circuits Using Digital Microfluidics* (Artech House, Norwood, MA, 2007).
[22] W.-C. Tian and E. Finehout, *Microfluidics for Biological Applications* (Springer, New York, 2008).
[23] M. Queralt-Martín, M. Pradas, R. Rodríguez-Trujillo, M. Arundell, E. Corvera Poiré, and A. Hernández-Machado, Phys. Rev. Lett. **106**, 194501 (2011).
[24] B. Jha, L. Cueto-Felgueroso, and R. Juanes, Phys. Rev. Lett. **106**, 194502 (2011).
[25] N. T. Nguyen and S. T. Wereley, *Fundamentals and Applications of Microfluidics*, Integrated Microsystems Series (Artech House, Norwood, MA, 2006).
[26] B. Derjaguin and M. Kusakov, Izv. Akad. Nauk. SSSR, Ser. Khim. **5**, 741 (1936).
[27] F. Brochard-Wyart, J. M. Di Meglio, D. Quere, and P. G. De Gennes, Langmuir **7**, 335 (1991).
[28] C. Bauer and S. Dietrich, Phys. Rev. E **62**, 2428 (2000).
[29] G. O. Berim and E. Ruckenstein, J. Phys. Chem. B **108** (2004).
[30] K. B. Glasner and T. P. Witelski, Phys. Rev. E **67**, 016302 (2003).
[31] J. A. Diez and L. Kondic, Phys. Fluids **19**, 072107 (2007).
[32] M. B. Gratton and T. P. Witelski, Phys. Rev. E **77**, 016301 (2008).
[33] G. J. Merchant and J. B. Keller, Phys. Fluids **4**, 477 (1992).
[34] X. Zhang, P. Neogi, and R. M. Ybarra, J. Colloid Interface Sci. **249**, 134 (2002).
[35] V. A. Lubarda and K. A. Talke, Langmuir **27**, 10705 (2011).
[36] M. E. Diaz, J. Fuentes, R. L. Cerro, and M. D. Savage, J. Colloid Interface Sci. **348**, 232 (2010).
[37] J. M. Gomba and G. M. Homsy, Langmuir **25**, 5684 (2009).
[38] A. Oron, S. H. Davis, and S. G. Bankoff, Rev. Mod. Phys. **69**, 931 (1997).
[39] P. G. de Gennes, F. Brochard-Wyart, and D. Quéré, *Capillarity and Wetting Phenomena: Drops, Bubbles, Pearls, Waves* (Springer, New York, 2004).
[40] L. W. Schwartz and R. R. Eley, J. Colloid Interface Sci. **202**, 173 (1998).
[41] C. A. Perazzo and J. Gratton, J. Fluid Mech. **507**, 367 (2004).
[42] U. Thiele, M. Velarde, and K. Neuffer, Phys. Rev. Lett. **87**, 16104 (2001).
[43] A. Bertozzi, G. Grün, and T. Witelski, Nonlinearity **14**, 1569 (2001).
[44] A. J. Tanasijczuk, C. A. Perazzo, and J. Gratton, Euro. J. Mech. B **29**, 465 (2010).
[45] J. M. Gomba, Phys. Rev. E **85**, 056701 (2012).